UNIVERSITY OF LEEDS

This is a repository copy of *Homogeneous coating of photonic macroporous oxides with inorganic nanocrystals*.

White Rose
university consortium
Universities of Leeds, Sheffield & York

eprints@whiterose.ac.uk
https://eprints.whiterose.ac.uk/

COMMUNICATION

Homogeneous Coating of Photonic Macroporous Oxides with Inorganic Nanocrystals

Robert Mitchell,[a] Rik Brydson[b] and Richard E. Douthwaite*[c]

This Article is Published in Celebration of the 50th Anniversary of the Opening of the Chemistry Department at the University of York

A simple method to obtain homogeneous sub-monolayer coverage of metal oxide and chalcogenide nanocrystals onto porous oxide supports is described. Quantitative nanoparticle coverage was probed using photonic macroporous oxide supports. Composites of nanocrystals of TiO_2, Fe_3O_4 or CdS dispersed onto macroporous SiO_2 or ZrO_2 all show a predictable linear shift in the photonic stop band position.

The development of methods for the systematic construction of materials is necessary for the rational implementation of function. For widespread application, simple and scalable methods are required. Materials comprising, or incorporating, nanoparticles have applications based on their unique size-dependent physical and chemical properties and high surface area to volume ratio. To avoid compromising performance, it is therefore important to avoid nanoparticle aggregation and sintering.[1] In solution, surface ligand (steric) or electrostatic stabilisation is typically used to prevent aggregation and precipitation, whereas in the solid state dispersion on a stable, non-interacting support is required.[1]

A further challenge is to develop synthetic methodologies that incorporate nanoparticles with controlled shape and size, which are distributed homogeneously throughout a porous substrate. In-situ nanoparticle formation and coating using vapour deposition techniques or soluble metal salts do not typically allow control of nanoparticle shape and size and usually lead to a heterogeneous distribution.[2] Alternatively, ligand-stabilised nanoparticles with pre-formed shape and size can be prepared independently for subsequent deposition onto a substrate, and there are several examples using metal nanoparticles (principally gold) for catalytic and analytical applications.[3] However, it is still necessary to avoid nanoparticle aggregation during deposition or post-synthesis processing, particularly as the nanoparticle loading increases.

To control nanoparticle dispersion, surface treatments such as silylation have been developed for porous ceramic monoliths that increase the nanoparticle to substrate hydrophobic interaction,[4] and specific bonding interactions such as disulphide linkages to anchor Au nanoparticles.[3b, 5] All these studies are limited to metal nanoparticles supported on monoliths for principally catalytic and analytical applications and typically use metal loadings < 5 wt%.

To the best of our knowledge there are no general procedures for obtaining high loadings (ca. >10 wt %) of semiconductor nanocrystals on porous solids that result in homogeneous coverage. Herein, we describe a very simple procedure for quantitatively depositing nanocrystals of binary oxide and chalcogenides into porous oxides. Specifically, ordered macroporous oxides have been chosen because in addition to electron microscopy techniques, the distribution of the nanoparticles can be examined by measuring the optical properties of the macroporous substrate and their nanoparticle composites. Whilst the coverage of planar surfaces is ubiquitous in materials chemistry, bulk assessment of homogeneous coverage is far from straightforward. Ordered macroporous materials are of significant interest because of their optical properties as three dimensional photonic crystals.[6] Light manipulation by these materials has application including emission tuning[7] and laser resonators,[8] and the enhancement of photocatalytic reactions[9] and photon-to-electron conversion of photoelectrodes.[10]
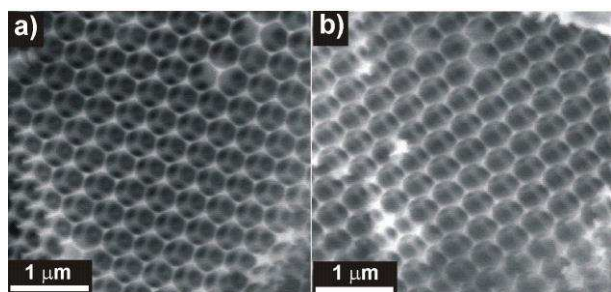
Figure 1. a) SEM image of *mac*-SiO₂; b) SEM image of 60 wt% *nan*-TiO₂@*mac*-SiO₂.

Figure 2. a) DRUVS of *nan*-TiO₂@*mac*-SiO₂ as a function of *nan*-TiO₂ loading; b) shift in λ_{max} of the stop band centred at 700 nm as a function of *nan*-TiO₂ loading.

A characteristic feature of photonic materials is stop bands which represent wavelengths that cannot propagate through the photonic medium. Stop bands of many materials can be conveniently measured using diffuse reflectance UV-Vis spectroscopy (DRUVS) and the position is dependent on several parameters including the modulation of the refractive index between the material and the voids (*vide infra*).[6a, 11] The coating method described here allows the predictable modification of photonic properties and integration of functional nanoparticles to give composites that could have application in a range of photonic and chemical technologies.

Ordered macroporous materials were prepared using a modified literature procedure from a polystyrene sphere template, which was impregnated with a soluble precursor, followed by calcination in air.[12] This method allows control of the pore size, although thermal shrinkage ultimately gives pores that are smaller than the template. Initially, macroporous silica (mac-SiO2) derived from 500 nm polystyrene spheres was prepared and scanning electron microscopy (SEM) shows a 420 nm periodic array of voids commensurate with an inverse opal structure (Figure 1a). DRUVS of a powdered sample shows two intense stop bands at 700 and 425 nm (Figure 2a), which correspond to the 111 and 220 optical Bragg reflections, and consequently *mac*-SiO2 appears red in reflected white light and green in transmission, respectively.[6a] Powder X-ray diffraction (PXRD) shows that the walls comprise amorphous SiO2.
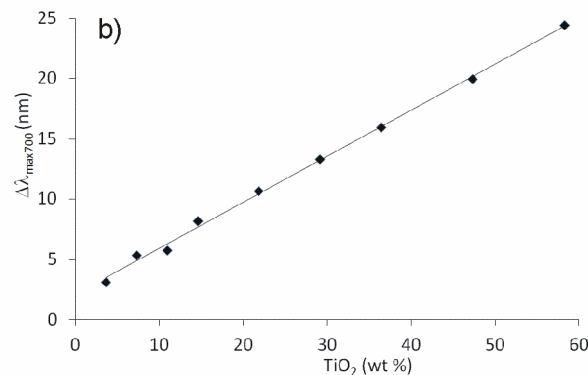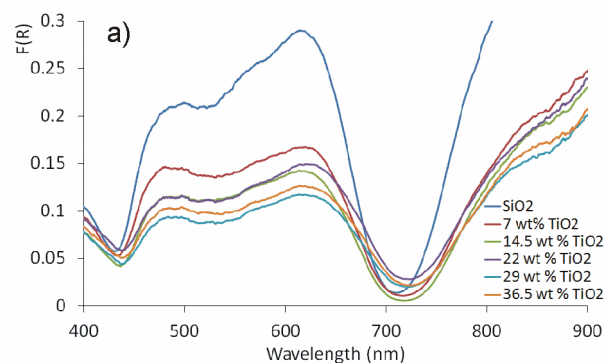
Nanocrystals of titanium dioxide (*nan*-TiO₂) were prepared using a hydrothermal method with oleic acid as the surface stabilising ligand.[13] Transmission electron microscopy (TEM) (Figure 3a) and PXRD showed that the nanoparticles are on average 8.9 ± 1 nm in diameter, single crystalline and exhibit the anatase phase. Combustion analysis gave an oleic acid:TiO₂ molar ratio of 1.25:1 and the nanocrystals can be dispersed in common organic solvents to give optically transparent solutions.

In order to obtain sub-monolayer coverage of *mac*-SiO₂ with *nan*-TiO₂, target loadings were selected based on the measured (BET) surface area of *mac*-SiO₂ (91 ± 1 m²g⁻¹) and estimation of the area of a single *nan*-TiO₂ particle obtained from TEM imaging. Calculation (see the Supporting Information) showed that a loading of 50 wt% of *nan*-TiO₂ gives an estimated coverage of *mac*-SiO₂ of *ca.* 20 %, and would give a measurable change in the DRUVS stop band position (*vide infra*). In this study nanoparticle loadings of between 4 and 60 wt% have been investigated for *mac*-SiO₂.
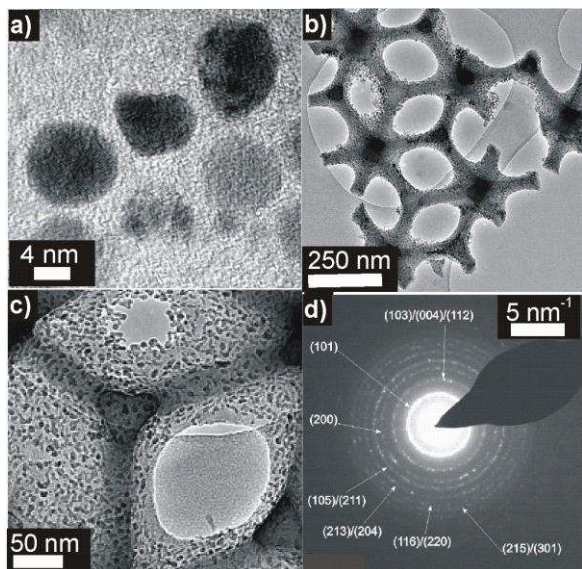
Figure 3. a) TEM image of *nan*-TiO₂; b) and c) TEM image of 60 wt% *nan*-TiO₂@*mac*-SiO₂; d) SAED of *nan*-TiO₂@*mac*-SiO₂.

Deposition of the nanocrystals was initially attempted by simply evaporating a hexane or chloroform solution of the nanocrystals containing a suspension of *mac*-SiO₂. SEM showed that after calcination at 500 °C for 5 hr the *nan*-TiO₂ had aggregated to give a largely phase separated composite and that some of the macropores were occluded with the *nan*-TiO₂ aggregates (Figure S3c). The interaction between *nan*-TiO₂ and *mac*-SiO₂ is therefore insufficient to drive adsorption, however if the *nan*-TiO₂/*mac*-SiO₂ interaction is irreversible, local concentrations of nanocrystals are also likely to be observed. Thus there is a requirement for optimisation of the adsorption-desorption equilibria between the nanocrystals, the solvent medium, and the porous support. To increase the interaction between *nan*-TiO₂ coated with oleic acid and *mac*-SiO₂, the surface of *mac*-SiO₂ was modified to increase the lipophilicity. A range of hydrocarbylsilanes and fatty acids, which react with surface hydroxide groups and are covalently bound to the silica surface, were investigated at a series of concentrations. Solvents of varying polarity were also investigated ranging from water to hexane.

After optimisation, it was found that coating *mac*-SiO₂ with oleic acid and adding oleic acid to a chloroform solution of *nan*-TiO₂, gave a homogeneous distribution of *nan*-TiO₂ in *mac*-SiO₂ (*nan*-TiO₂@*mac*-SiO₂). Removal of the oleic acid ligands and residual solvent on calcination at 500 °C gave *nan*-TiO₂@*mac*-SiO₂ with no evidence of *nan*-TiO₂ aggregation or agglomeration as initially judged by SEM comparison of *mac*-SiO₂ and *nan*-TiO₂@*mac*-SiO₂, which are essentially indistinguishable (Figure 1b). The composites are chemically robust to dissolution of the *nan*-TiO₂ nanocrystals or their aggregation in water or common organic solvents. TEM clearly shows that the surface of *mac*-SiO₂ is decorated with particles commensurate with *nan*-TiO₂ (Figure 3b and c). Sub-monolayer coverage is evident and a tilt

series of TEM micrographs and elemental mapping (using Scanning TEM (STEM)/ energy dispersive X-ray analysis (EDX)) (Figure S4a) indicates that the surface of the macropores is homogeneously decorated with *nan*-TiO₂ with no evidence of localised concentration. TEM selected area electron diffraction (SAED) (Figure 3d) confirm that the particles are the anatase polymorph of TiO₂, which is also supported by PXRD (Figure S5b). EDX gave a Ti:Si elemental ratio consistent with the target loading of 60 wt%.

DRUVS data of 4 - 60 wt% loaded *nan*-TiO₂@*mac*-SiO₂ showed that the stop bands are red shifted to longer wavelengths (Figure 2a) with respect to *mac*-SiO₂, and that the shift is directly proportional to the loading (Figure 2b). The relationship between the stop band maximum (λ_{max}), the relative refractive indices (n) of the void and wall materials, the macroporous lattice plane spacing (d_{hkl}), the volume wall fill factor (φ), and the Bragg plane order (*m*), is shown in Equation

$$\lambda_{max} = \frac{2d_{hkl}}{m} \left[\varphi n_{wall} + (1 - \varphi)n_{void} \right] \tag{1}$$

(1).[6a]

A red shift of λ_{max} is commensurate with the addition of a material with a greater refractive index than the materials that comprise the existing wall or voids (n = 2.49 (TiO₂), 1.45 (SiO₂) and 1.00 (air), respectively). The addition of a third component to the macroporous structure modifies Equation (1) to give Equation (2), where χ is the volume fraction of TiO₂.

$$\lambda_{max} = \frac{2d_{hkl}}{m} \left[\varphi n_{SiO2} + \chi n_{TiO2} + (1 - \varphi - \chi)n_{void} \right] \tag{2}$$

In the absence of significant dispersion and scattering effects, the two most intense stop bands at 425 and 700 nm are expected to exhibit different shifts of λ_{max} as a function of loading, which is reflective of the ratio of the interplanar spacing d_{220}/d_{111} = 0.612.[6a] The ratio of the gradients of the lines of least squares fit for the shift in λ_{max} at the bands centred at 425 and 700 nm is 0.18/0.28 = 0.64 which is in good agreement and confirms the Bragg reflection assignments. The filling factor, φ, for *mac*-SiO₂ without *nan*-TiO₂ can be calculated from Equation (1) or (2) and gives φ = 4.9 %, which is similar to reported examples of macroporous silicas.[6a] The addition of *nan*-TiO₂ gives a linear increase in the total fill factor ($\varphi + \chi$) to a maximum value of 7.1 % for the 60 wt% loading, and a change in λ_{max} ($\Delta\lambda_{max}$) = 24 nm indicating that the majority of the volume in these materials is void, as shown by the SEM and TEM images. In addition the intensity of the stop band is not significantly reduced on progressively increasing the titania loading indicating that the coverage of the *nan*-TiO₂ particles is homogeneous. For materials where agglomeration or aggregation of TiO₂ occurred the stop band intensity was observed to be significantly broadened and reduced.

The deposition methodology is also applicable to other nanoparticles and porous oxides. For example, oleic acid stabilised nanocrystals of Fe₃O₄ (*nan*-Fe₃O₄)[14] (size 5-10 nm) or oleic acid stabilised nanocrystals of CdS (*nan*-CdS)[15] (size 2-5

nm) were also deposited onto *mac*-SiO₂. For the *nan*-CdS composites removal of the stabilising ligands and oleate moieties was achieved under an argon atmosphere to prevent CdS oxidation. SAED and PXRD indicated the retention of the nanocrystal structure, and microscopy showed homogeneous coating analogous to *nan*-TiO₂@*mac*-SiO₂, for example as shown by elemental mapping for *nan*-Fe₃O₄@*mac*-SiO₂ (Figure 4). The DRUVS data of *nan*-Fe₃O₄@*mac*-SiO₂ again exhibited a red shift (Figure S6b) of λ_{max} proportional to the nanocrystal loading. The slope is commensurate with an increase in the refractive index of the macroporous structure (n = 2.40 (Fe₃O₄)), to give an increase in the total filling factor, and shifts of λ_{max} very similar to that of *nan*-TiO₂@*mac*-SiO₂.
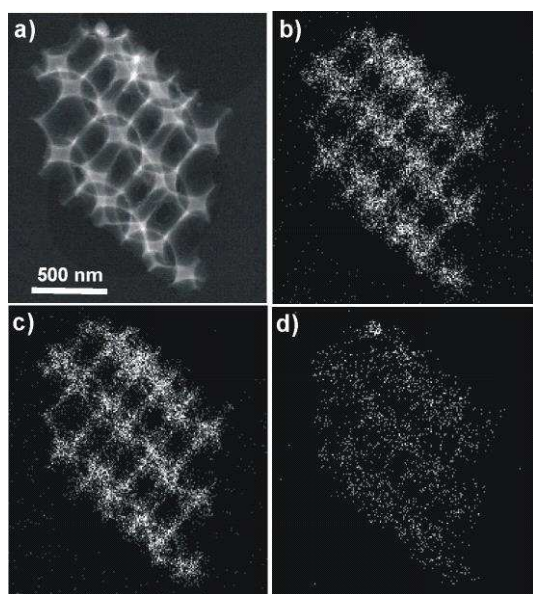

Figure 4. Scanning TEM EDX of 33 wt% *nan*-Fe₃O₄@*mac*-SiO₂ a) TEM image, b) Oxygen map, c) Silicon map, d) Iron map.

Furthermore, other macroporous oxides can be similarly decorated, for example, *mac*-ZrO₂ to give *nan*-TiO₂@*mac*-ZrO₂ and *nan*-Fe₃O₄@*m*-ZrO₂. In contrast to *mac*-SiO₂, which is formed from amorphous SiO₂, *mac*-ZrO₂ is composed of nanocrystalline tetragonal ZrO₂ (Figure S5e). Scherrer analysis of the PXRD data of *mac*-ZrO₂ typically gave a calculated crystallite size of 5 nm indicating that the macroporous support and impregnated nanoparticles are of comparable size. For *mac*-ZrO₂ (n = 2.20) derived from a 400 nm template a periodicity of 270 nm is observed, which exhibits one stop band, with λ_{max} = 490 nm for the 111 Bragg reflection. A filling factor φ = 7.2 % is calculated for *mac*-ZrO₂, which in comparison to *mac*-SiO₂ (φ = 4.9 %) is consistent with an increase in wall density and greater shrinkage in *mac*-ZrO₂. This is also reflected in the much lower surface area (20.6 ± 0.3 m²g⁻¹) of *mac*-ZrO₂ in comparison to *mac*-SiO₂ (91±1 m²g⁻¹).

Coating of *mac*-ZrO₂ with oleic acid allowed the homogenous decoration with *nan*-TiO₂ or *nan*-Fe₃O₄ as judged by the SEM and TEM data. Again, using the measured surface area an estimation of sub monolayer coverage suggested an upper limit of *ca*.30 wt % for *nan*-TiO₂ or *nan*-Fe₃O₄ nanoparticles. DRUVS data for a series of loadings between 4 and 27 wt% *nan*-TiO₂@*mac*-ZrO₂ gives a linear red shift of the stop band λ_{max}, where for example 27 wt% *nan*-TiO₂@*mac*-ZrO₂, gives $\Delta\lambda_{max}$ = 32 nm (Figure S6c). This gives a calculated total filling factor of 12.5 %, which is greater than for analogous *nan*-TiO₂@*mac*-SiO₂ composites because of the reduced pore size and periodicity of *mac*-ZrO₂.

Of note is the change in surface area on addition of nanoparticles to *mac*-SiO₂ and *mac*-ZrO₂. For example 10 wt% *nan*-TiO₂@*mac*-SiO₂, exhibits a reduced surface area of 83±1 m²g⁻¹ in comparison to *mac*-SiO₂, whereas for 10 wt% *nan*-TiO₂@*mac*-ZrO₂ a greater surface area of 29.3±0.3 m²g⁻¹ is observed in comparison to *mac*-ZrO₂. For dense, microcrystalline, *mac*-ZrO₂ the addition of *nan*-TiO₂ presumably increases the surface roughness and overall surface area, whereas for amorphous *mac*-SiO₂ the addition of *nan*-TiO₂ indicates that the nanoparticles are embedded into the surface blocking access to area within the amorphous walls.

Conclusions

Modification of the nanoparticle and substrate surfaces provides a very simple methodology for the homogenous deposition of metal oxide and metal chalcogenides on oxide supports. The surface coating and the solvent medium control the nanoparticle dispersion, and the nanoparticle/nanoparticle and nanoparticle/support interactions. On calcination isolated nanoparticles are obtained, which are in direct contact with the support. Microscopy and optical data show that for ordered macroporous supports the photonic properties are retained and that the stop band position can be predictably modified as a function of nanoparticle refractive index and loading. Indeed once a calibration curve has been determined, the loading of a macroporous material can be obtained simply by measuring spectroscopically the position of a stop band.

Notes and references

[a]Department of Chemistry, University of York Heslington, York, YO10 5DD (UK). E-mail: richard.douthwaite@york.ac.uk
[b] Institute for Materials Research, School of Process, Environmental and Materials Engineering, University of Leeds, Leeds LS2 9JT (UK)
†Electronic Supplementary Information (ESI) available: Synthetic procedures, SEM, TEM, EDX, PXRD, DRUVS and BET measurements. See DOI: 10.1039/c000000x/

1   G. Schmid, Nanoparticles, Wiley VCH, Weinheim, 2010.

2   a) R. J. White, R. Luque, V. L. Budarin, J. H. Clark and D. J. Macquarrie, Chem. Soc. Rev., 2009, **38**, 481; b) M. Santiago, A. Restuccia, F. Gramm and J. Perez-Ramirez, Micropor. Mesopor. Mat., 2011, **146**, 76.

3   a) N. F. Zheng and G. D. Stucky, J. Am. Chem. Soc., 2006, **128**, 14278; b) D. Connolly, B. Twamley and B. Paull, Chem. Commun., 2010, **46**, 2109.

4   S. H. Ding, W. P. Qian, Y. Tan and Y. Wang, Langmuir, 2006, **22**, 7105.

5   F. Pena-Pereira, R. Duarte and A. C. Duarte, Trac-Trends Anal. Chem., 2012, **40**, 90.

6   a) R. C. Schroden, M. Al-Daous, C. F. Blanford and A. Stein, Chem. Mat., 2002, **14**, 3305; b) J. I. L. Chen, G. von Freymann, S. Y. Choi, V. Kitaev and G. A. Ozin, Adv. Mater., 2006, **18**, 1915; c) F. Marlow, Muldarisnur, P. Sharifi, R. Brinkmann and C. Mendive, Angew. Chem. Int. Ed., 2009, **48**, 6212; d) L. Gonzalez-Urbina, K. Baert, B. Kolaric, J. Perez-Moreno and K. Clays, Chem. Rev., 2012, **112**, 2268.

7   a) J. Martorell and N. M. Lawandy, Phys. Rev. Lett., 1990, **65**, 1877; b) P. Lodahl, A. F. van Driel, I. S. Nikolaev, A. Irman, K. Overgaag, D. Vanmaekelbergh and W. L. Vos, Nature, 2004, **430**, 654.

8   a) J. P. Dowling, M. Scalora, M. J. Bloemer and C. M. Bowden, J. Appl. Phys., 1994, **75**, 1896; b) Y. Nishijima, K. Ueno, S. Juodkazis, V. Mizeikis, H. Misawa, M. Maeda and M. Minaki, Opt. Express, 2008, **16**, 13676; c) S. H. Kim, W. C. Jeong and S. M. Yang, Chem. Mat., 2009, **21**, 4993.

9   a) J. I. L. Chen and G. A. Ozin, J. Mater. Chem., 2009, **19**, 2675; b) M. Wu, Y. Li, Z. Deng and B. L. Su, ChemSusChem, 2011, **4**, 1481; c) L. W. Zhang, C. Baumanis, L. Robben, T. Kandiel and D. Bahnemann, Small, 2011, **7**, 2714.

10 a) S. Nishimura, N. Abrams, B. A. Lewis, L. I. Halaoui, T. E. Mallouk, K. D. Benkstein, J. van de Lagemaat and A. J. Frank, J. Am. Chem. Soc., 2003, **125**, 6306; b) S. Guldin, S. Huttner, M. Kolle, M. E. Welland, P. Muller-Buschbaum, R. H. Friend, U. Steiner and N. Tetreault, Nano Lett., 2010, **10**, 2303; c) X. Q. Chen, J. H. Ye, S. X. Ouyang, T. Kako, Z. S. Li and Z. G. Zou, ACS Nano, 2011, **5**, 4310.

11 S. Nishimura, A. Shishido, N. Abrams and T. E. Mallouk, Appl. Phys. Lett., 2002, **81**, 4532.

12 B. T. Holland, C. F. Blanford, T. Do and A. Stein, Chem. Mat., 1999, **11**, 795.

13 P. D. Cozzoli, A. Kornowski and H. Weller, J. Am. Chem. Soc., 2003, **125**, 14539.

14 A. Demortiere, P. Panissod, B. P. Pichon, G. Pourroy, D. Guillon, B. Donnio and S. Begin-Colin, Nanoscale, 2011, **3**, 225.

15 N. Li, X. Zhang, S. Chen, X. Hou, Y. Liu and X. Zhai, Mater. Sci. Eng: B, 2011, **176**, 688.